JMEPEG (2024) 33:2585–2598
https://doi.org/10.1007/s11665-023-08163-2

©ASM International
1059-9495/$19.00

TECHNICAL ARTICLE

Process-Controlled Domain Switching and Improved Ferroelectric Properties in Lanthanum-Modified Lead Zirconate Titanate Films

Anina Anju Balaraman, A. Antony Jeyaseelan, and Soma Dutta

Submitted: 18 October 2022 / Revised: 3 March 2023 / Accepted: 23 March 2023 / Published online: 13 April 2023

In the present study, the effect of processing parameters like annealing temperature, excess of lead (Pb) content, and film thickness on the crystallographic orientation, dielectric and ferroelectric properties of PLZT (Pb/La/Zr/Ti: 92/8/52/48) films are investigated. For the investigation, PLZT films were prepared on Pt/Ti/SiO_2/Si substrate by chemical solution deposition method and annealed at different temperatures (600, 625, 650, 675, and 700 °C). Diverse growth orientation was observed for different annealing temperatures that gave rise to modified electrical properties in the PLZT films. Comparative studies on processing temperature exhibited improved ferroelectric properties in 650 °C annealed PLZT film, which is attributed to its crystallinity (Full width at half maximum, $FWHM_{101}$ = 0.49°) and texture coefficient (γ = 0.832). Excess Pb content (3 wt.%) yielded improved ferroelectric properties in PLZT film with a ~ 10% increment in domain switching. The PLZT film with 3 wt.% Pb-excess content showed an ASTM class 5B adhesion on Pt/Ti/SiO_2/Si substrate, a nano-hardness value of 7894.43 MPa, and a Young's modulus value of 143.05 GPa. To further study the effect of process control parameters on PLZT film, variation of thicknesses (492, 768, and 1500 nm) was studied for 3 wt.% Pb-excess film. The study showed considerable domain switching (switching current = 58.10 μA at 40 kV/cm), improved dielectric constant (~ 2750), higher polarization (P_{max} = 71.4 $\mu C/cm^2$) at a low electric field 334 kV/cm and low leakage current for 1500 nm thick PLZT film. A total energy storage density of ~ 26 J/cm^3 at 1020 kV/cm and tunability of 68.46% at ~ 200 kV/cm was achieved for PLZT film with 3 wt.% excess Pb.

Keywords coating, energy, inorganic, PLZT film, process control

1. Introduction

The lead-based ferroelectric systems have superior dielectric, piezoelectric, and energy storage properties (Ref 1-26). Among those, the lanthanum-modified lead zirconate titanate (PLZT) $(Pb_{1-x}La_x)(Zr_{1-y}Ti_y)O_3$ systems have been extensively studied in recent years for microelectronics, microelectromechanical systems (MEMS), pulsed power capacitors, electro-optic applications, ferroelectric non-volatile memories (NV-FeRAMs), high density dynamic random access memories, infrared pyroelectric detectors, decoupling capacitors, microsensors, etc., due to their exceptional dielectric, piezoelectric, and electro-optic characteristics (Ref 1, 27-31). The elementary operation of these ferroelectric devices is solely based on their polarization switching in response to external factors such as temperature, stress, and electric field (Ref 32). These switching studies are essential to understand the functionality of every ferroelectric system. For instance, the primary determinant of read/write operations in NV-FeRAMs is polarization switching (Ref 33).

Designing ferroelectric devices for specific applications requires careful consideration of process temperature (Ref 34) since it influences the ferroelectricity of the system. The study on the perovskite $CH_3NH_3PbI_3$ film by F. Wang et al. reports altered crystallinity and crystal size, causing different domain behaviors at different annealing temperatures (Ref 35). In the HfO_2:SiO_2 thin films, a significant process temperature dependence of the remnant polarization, breakdown field, and leakage current densities was reported (Ref 36). In addition, a decrease and an increase in the remnant polarization and the coercive electric field, respectively, were observed in sol–gel deposited BFO thin films with increasing annealing temperature (550–650 °C) (Ref 37). Previous other studies have also shown that the presence of excess lead (Pb) content and annealing temperature can greatly change the electrical characteristics by changing the microstructural properties such as nucleation, perovskite growth, crystalline orientation, grain size, and shape of PLZT films (Ref 27, 38-43). Additionally, numerous researches confirm that the properties of films change with their thickness as well (Ref 30, 44-51). The phenomenological theory has been used to conceptually explain the switching kinetics in ferroelectrics (Ref 52-54). These kinetics have then been experimentally explored by measuring switch-

Anina Anju Balaraman and **Soma Dutta**, Materials Science Division, CSIR-National Aerospace Laboratories, Bangalore 560017, India; and Academy of Scientific and Innovative Research (AcSIR), Ghaziabad 201002, India; and **A. Antony Jeyaseelan**, Materials Science Division, CSIR-National Aerospace Laboratories, Bangalore 560017, India; and Centre for Nano Science and Engineering, Indian Institute of Science, Bangalore 560012, India. Contact e-mail: som@nal.res.in.

ing current transients or by analyzing domain motions (Ref 55-57).

Although the ferroelectric properties of PLZT system are well known, no literature reports the combined effect of various processing parameters on the crystallographic orientation causing the variation in dielectric and ferroelectric properties of PLZT films. As the Pb volatilization and/or Pb diffusion into the bottom substrate during the heat treatment disrupts the stoichiometry of the system and results in the formation of non-ferroelectric pyrochlore phase (Ref 38, 39, 41), the processing temperature is lowered/adjusted to minimize the Pb volatility (Ref 39). Furthermore, definite amount of Pb-excess contents are also added to the precursor solution to maintain its stoichiometry (Ref 40). Considering the above facts, the effect of process control parameters (like Pb-excess content in the composition, annealing temperature and thickness of the film) on physical (structure, microstructure, mechanical) and functional properties (ferroelectric properties and domain switching) of PLZT film (La/Zr/Ti = 8/52/48) is investigated thoroughly in the present study. The PLZT composition chosen for the study is the best composition reported by many for dielectric and ferroelectric properties (Ref 58-61). There are various film deposition techniques available for PLZT films; this paper reports the process control parameters associated with Chemical Solution Deposition (CSD) of the film considering its advantages of cost effectiveness, excellent control over stoichiometry and non-availability of such reports.

2. Experiments

The precursor solution for the PLZT composition of molecular formula $(Pb_{0.92}La_{0.08})(Zr_{0.52}Ti_{0.48})O_3$ (PLZT) was prepared chemically as reported earlier with different Pb-excess content (0, 1, 2, 3, and 5 wt.%) (Ref 29, 62). The precursor solution was then spin-coated on Pt (111)/Ti/SiO_2/Si substrates at an rpm of 6500 for 30 s, followed by two-step pyrolysis at 500 and 650 °C to remove the organics. In spite of the fact that Pt-coated Si substrates have more fatigue properties than oxide electrodes, Pt/Ti/SiO_2/Si substrates were used in the study due to their high electrical conductivity, high chemical resistance, and wafer scalability (Ref 63). The spinning and pyrolysis process was repeated until the desired thickness is achieved. Three different thicknesses (492, 768, and 1500 nm) were prepared to study the thickness effect on the microstructure and electrical properties of the PLZT film. All the PLZT films of different Pb-excess contents were annealed at 600, 625, 650, 675, and 700 °C, for 30 min in the air atmosphere. The PLZT films with 0, 1, 2, 3, and 5 wt.% Pb-excess contents are named PLZT0, PLZT1, PLZT2, PLZT3, and PLZT5, respectively. Electrode layer (Ag) at the top of the film was deposited in a circular dot pattern of 0.3 mm diameter using a physical mask while thermal vapor deposition. A typical schematic representation of the thin film stack is given in Fig. 1. The XRD (X-pert, Copper_k_α, λ = 1.54 Å) of the thin film samples were taken to investigate the phase formation and crystal structure. The microstructure of the films was studied through FESEM (SEM, Carl Zeiss supra 40 VP with Gemini column) images and thickness was measured by Dektak XT surface profilometer. The dielectric, piezoelectric and ferroelectric property measurements were carried out using thin-film analyzer (aixACCT FE 2000).

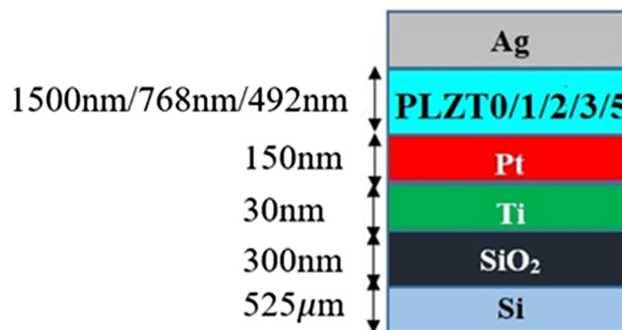

Fig. 1 Schematic representation of the metal/ferroelectric/metal stack structure of PLZT films under investigation

Once the process parameters are optimized for the improved ferroelectric properties, the mechanical properties of the film were also studied by nano-hardness test and cross-hatch adhesion test. Nano-hardness measurements of PLZT film (1500 nm thick) was carried out using a diamond indenter in NHT S/N: 04-00,114 instrument. The data acquired under linear loading mode, with a maximum applied load of 3.00mN. The provided loading and unloading rate was 6.00 mN/min with a pause time of 2 s. Five indents were made on each samples to measure the average hardness and Young's modulus values. For the ASTM D3359 adhesion test, a cross-hatch cutter (Elcometer 107) having 11 metal blades of 1 mm apart was chosen. Even cuts of 1 mm apart were made on the samples by scraping the cutter through the samples with sufficient pressure, ensuring the cutting edge hits the substrate. The film was then softly brushed to remove the possible detached flakes. Additional cuts were made at 90° to the previous cuts, followed by soft brushing. A pressure-sensitive tape was then placed over the engraved grid region, ensuring not to entrap air under the tape. The tape was then smoothly rubbed using fingers to establish uniform and firm contact between the tape and coating. The tape was then removed at an angle of 180° and the grid area is inspected under an optical microscope (Unitron) at 5X magnification.

3. Experimental Results

3.1 XRD Pattern Analysis

Figure 2(a)-(e) shows the low glancing angle (1 °C) XRD θ-2θ scans of the PLZT films having different Pb-excess content and annealed at different temperatures. All the PLZT films exhibited the tetragonal perovskite phase of PLZT crystal with no secondary phase and are in good agreement with the JCPDS card no: 00-046-0504. To compare the growth orientation in each films, the texture coefficient (γ) is calculated using the equation below (Ref 64, 65).

$$\gamma = \frac{I_{hkl}/I_{0\,hkl}}{1/N\left(\sum_{1}^{N} I_{hkl}/I_{0\,hkl}\right)} \quad \text{(Eq 1)}$$

where I_{hkl} represents the intensity of XRD peak measured from the plot, $I_{0\,hkl}$ represents the standard intensity value of PLZT powder sample, taken from JCPDS card number 00-046-0504 for particular (hkl) plane, and N represents the number of

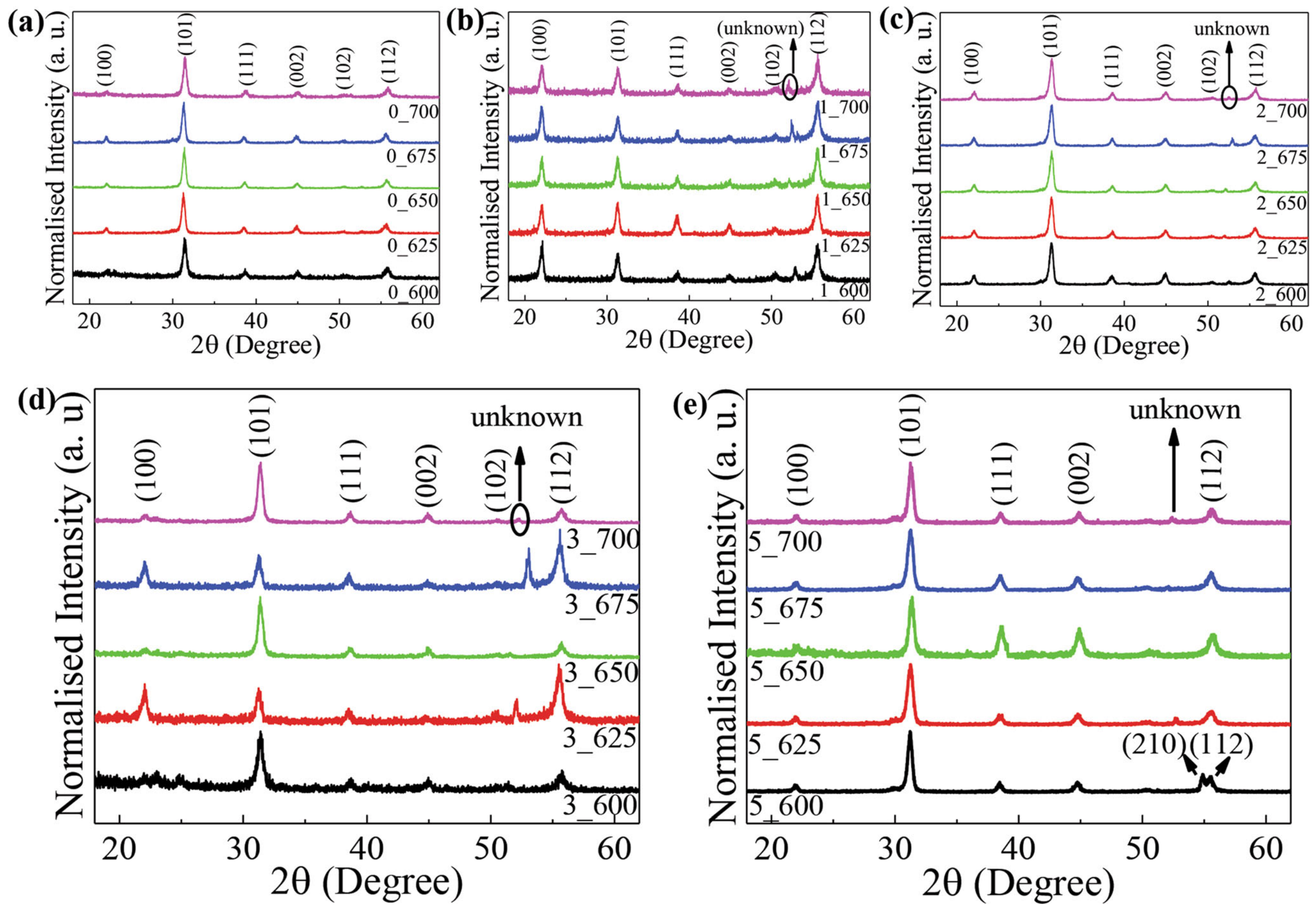

Fig. 2 XRD patterns of PLZT films, annealed at different temperatures (a) PLZT0, (b) PLZT1, (c) PLZT2, (d) PLZT3, and (e) PLZT5 films

diffraction peaks. The calculated texture coefficient value of each film is compared with their corresponding full-width half maximum (FWHM) value in Fig. 3(a)-(e).

From the above figures, it is observed that the films annealed at 650 °C shows higher γ value and lower FWHM which is desirable for directional orientation and better crystallinity (Ref 66-68). In PLZT film with no Pb-excess content, the γ value increased with increase in annealing temperature indicating maximum orientation along (101) direction, when the film is annealed at 650 °C (Fig. 3a). The 650 °C annealed PLZT0 film is the best because of its low full-width-half-maximum (FWHM = 0.49°) and high texture coefficient (γ = 0.83) values. All the PLZT1 films show low γ values, between 0.1 and 0.2 (Fig. 3b). It implies lack in particular orientation, which is desired. This leads to the lower functional properties of these films. Furthermore, all PLZT1 films showed high FWHM values. Hence, this set of films were not considered for further study. The PLZT2 films (Fig. 3c) show low FWHM and high γ. But due to the presence of the extra peak (at 2θ = ∼ 52°), the XRD pattern does not match with the reported literature. Therefore, this set of films were discarded from further studies. From Fig. 3(d), it is verified that the 650 and 700 °C annealed PLZT3 films show low FWHM and high γ values. Therefore, these film samples were further studied for electrical property measurements. For PLZT5 films, the 700 °C annealed film shows highest γ and lowest FWHM value (Fig. 3e). But due to the presence of the extra peak (at 2θ = ∼ 52°), the XRD pattern does not match with the reported literature. The same extra peak is also observed for 625, and 675 °C annealed films. Among this batch, the 650 °C annealed film was considered for further electrical studies due to its higher γ and low FWHM values compared to 600 °C annealed film.

The XRD spectra are further studied to calculate the intensity ratio of (111) peak to the maximum intensity peak (101) in PLZT0, PLZT3, and PLZT5 films, using the following expression:

$$\frac{I}{I_{max}} = \left(\frac{I_{(111)}}{I_{(101)}}\right) \times 100\% \quad \text{(Eq 2)}$$

The I/I_{max} ratio for (111) peak in PLZT0 films annealed at 600, 650, and 700 °C is 25, 16.5, 18.5%, respectively. This shows that the growth is more uniform towards (101) direction in PLZT0 film annealed at 650 °C and is consistent with the highly crystalline nature of the film obtained from the XRD results. However, as the Pb-excess content is raised to 5 wt.% (PLZT5_650), the I/I_{max} ratio for (111) peak is increased to ∼ 52%, indicating mixed orientation. Such a mixed orientation in PLZT5_650 film can adversely affect the electrical properties (Ref 50, 69). To gain a deeper understanding on the crystallographic orientation of the films, Rietveld refinement is carried out using the tetragonal phase of P4mm space group (CIF file no: 1521044). The obtained lattice parameters are listed in Table 1. No peak shift is observed in the XRD patterns of prepared PLZT films. Here, the residual stress is insignificant on the films as they are much thicker (∼ 1500 nm) than the critical thickness (Ref 70).

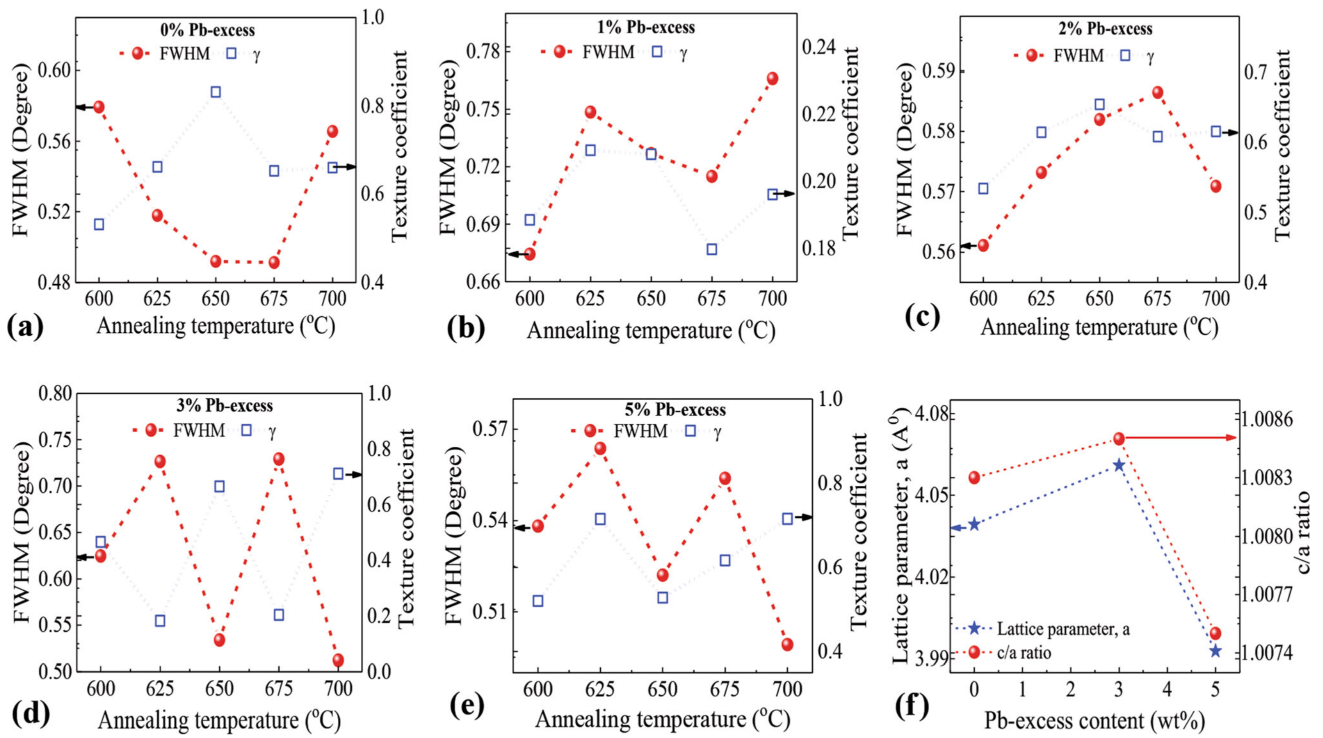

Fig. 3 FWHM & texture coefficient of PLZT film as calculated from XRD pattern (Fig. 1) (a) PLZT0, (b) PLZT1, (c) PLZT2, (d) PLZT3, and (e) PLZT5 film, and (k) lattice parameter & c/a ratio of PLZT films plotted against excess Pb content

Table 1 Rietveld refinement parameters of PLZT films

Pb-excess, wt.%	Annealing temperature, °C	Lattice parameters				Bragg R factor	R_p	R_{wp}	R_{exp}	Chi^2
		a, A°	c, A°	c/a ratio	Volume $(A°)^3$					
0	600	4.049880	4.108425	1.01446	66.7384	32.1	80	66.7	644	0.0107
	650	4.057312	4.097206	1.00983	67.447	28.1	54.1	52.9	740	0.0050
	700	4.032500	4.07690	1.01101	66.294	0	.	.	.	0
3	600	4.066554	4.018905	0.98828	66.460	42.3	87.9	73.4	595	0.0152
	650	4.062856	4.076957	1.00347	67.298	41.4	74.9	65.3	702	0.0086
	700	4.046700	4.040900	0.99857	66.173	32.8	64.7	61.3	698	0.0077
5	600	4.068207	4.113394	1.01110	68.078	33.8	52.9	53.6	679	0.0062
	650	4.050038	4.092078	1.01038	67.122	30.2	61.8	60.3	555	0.0118
	700	4.017084	4.060714	1.01086	65.528	28.4	53	54.5	689	0.0063

3.2 FESEM Image Analysis

The surface morphology of PLZT_650, PLZT3_650, and PLZT5_650 films was investigated using FESEM (Fig. 4a-c). All films exhibited a dense crack-free microstructure. The film thickness obtained from cross-sectional view is 1.5 μm for the cumulative layers (Fig. 4d). Further, the grain size and percentage of porosity of all the films were calculated using ImageJ software from the FESEM images and plotted against the Pb-excess content (Fig. 4e). The least percentage of porosity is observed in the PLZT3_650 film and might have contributed to the improvement in ferroelectric properties (Ref 27, 42, 43, 71).

3.3 Hysteresis Loops

Figure 5a represents the room temperature bipolar PE loops (frequency 100 Hz) of PLZT0 films annealed at different temperatures. PLZT0_650 film shows maximum polarization (P_{max}) 65.8 μC/cm^2 at 334 kV/cm. This is in good agreement with the enhanced crystallinity of the film verified using the XRD results (Fig. 3a). Similar enhancement in the polarization value is noted in PLZT3 film, when annealed at 650 °C (Fig. 5b). Therefore, PE-loop parameters of different Pb-excess films annealed at 650 °C are studied (Fig. 5c). In addition, the effect of annealing temperature, Pb-content, and thickness on the coercive field (E_c), remnant polarization (P_r), maximum polarization (P_{max}), and hysteresis loss (W_{loss}) are shown in Fig. 6.

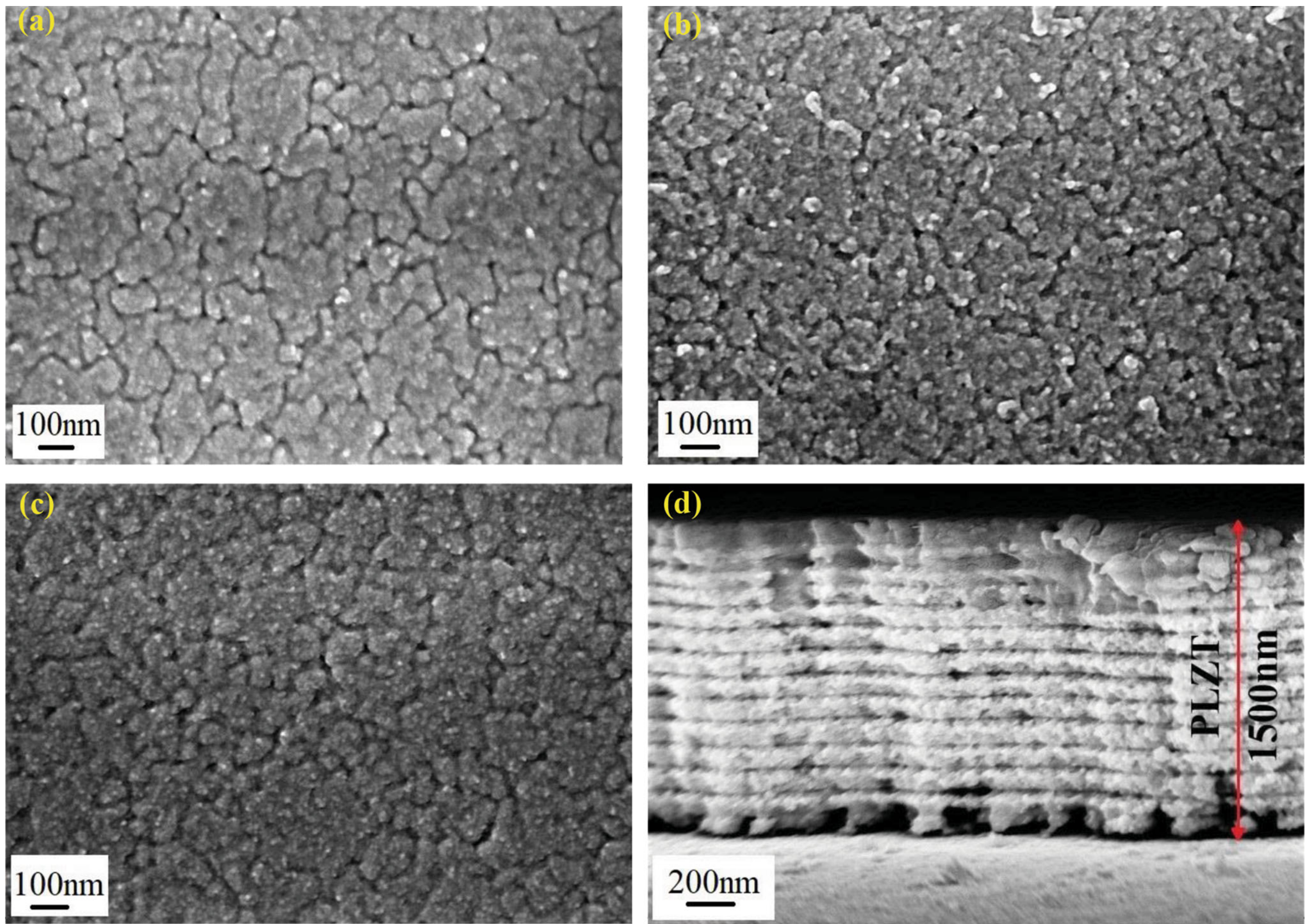

Fig. 4 FESEM images of (a) PLZT0_650, (b) PLZT3_650, and (c) PLZT5_650 film. Figure 3(d) is the cross-sectional view of PLZT3_650, and (e) plots the grain size and porosity of the PLZT films with Pb-excess content

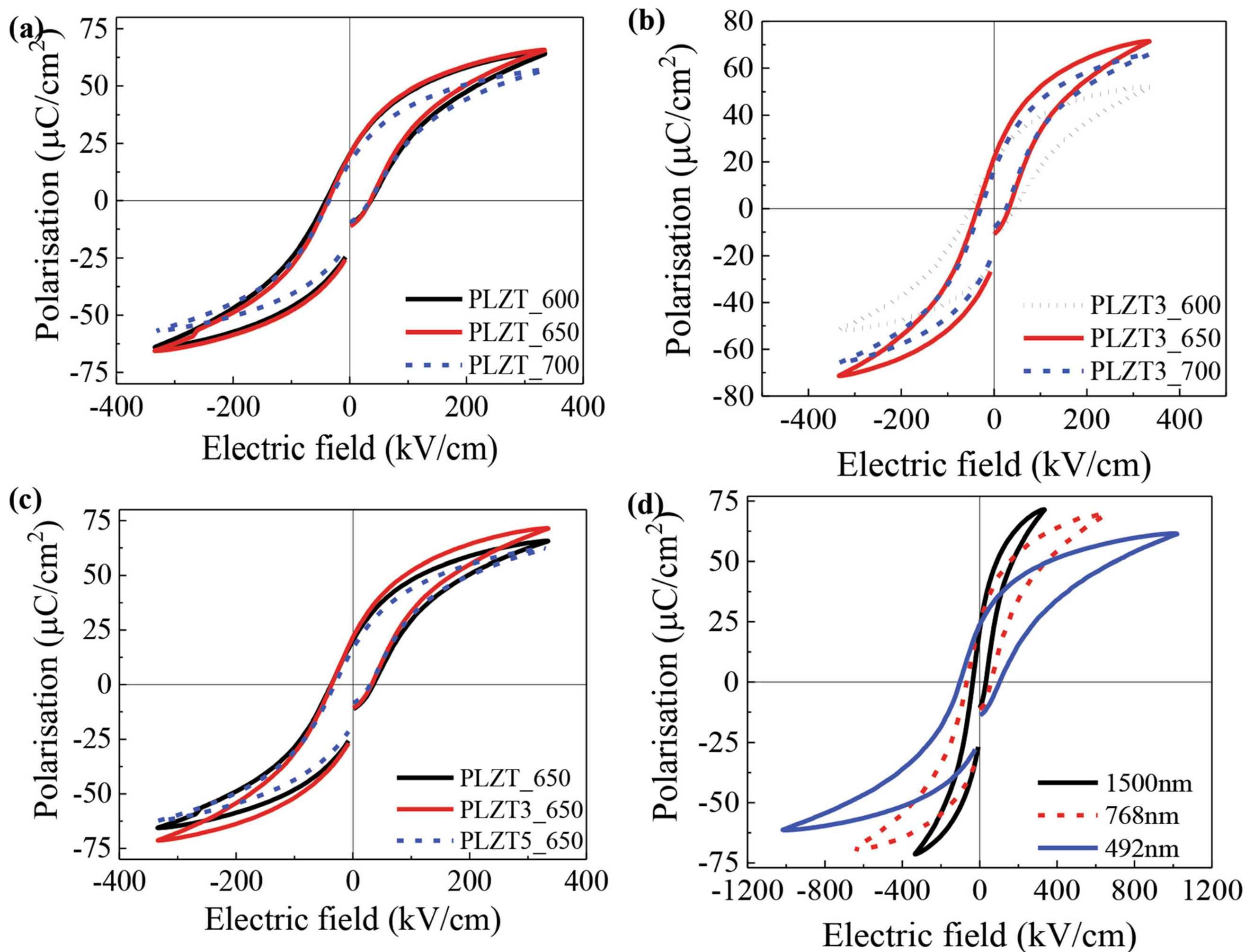

Fig. 5 Effect of process parameters on the room temperature PE hysteresis loops of PLZT films; (a) annealing temperature on PLZT0, and (b) PLZT3 films, (c) effect of Pb-excess, and (d) effect of thickness

Figure 6(a) and (b) depicts the P_r, P_{max}, E_c, and W_{loss} of PLZT0 film as a function of annealing temperature. The PLZT0 film annealed at 650 °C showed optimum P_{max} value, lower E_c, and reduced W_{loss}. The reduced E_c value in the film indicates better domain switching at lower electric fields. The P_{max} value reduction in the film annealed at 700 °C is due to the reduced crystalline quality of the film, as verified in the XRD analysis. In fact, the enhanced P_{max} in PLZT0__650 film arises from the highly crystalline nature, which is consistent with the XRD results (Fig. 3a). The PLZT0_650 film, which exhibited the best ferroelectric properties, is then compared with other Pb-excess films (PLZT3_650 & PLZT5_650) to find the optimum composition (Fig. 6c, d). This comparison shows a higher P_{max} of 71.4 μC/cm^2 for PLZT3_650 film, which is attributed to the improved density and crystallinity of this film, as discussed before (Fig. 4e, 3d). It is reported that higher density increases the volume fraction of polarization domains (Ref 72). The variation of P_r value with different Pb-excess content (Fig. 6c) may also be associated with c/a ratio variation (Fig. 3f) (Ref 73). Furthermore, there is a gradual reduction in the E_c values as the Pb content increases. This can be attributed to the backfield effects that act on domain walls during domain switching (Ref 74). In an externally applied electric field, the backfields may work against the switching of domains. In contrast, the backfield favors domain switching in the absence of an external electric field. This can be further explained with the help of surface morphology. The grain size in the films increases with an increase in Pb-excess content and, thereby, reduces both grain boundary density and domain wall density (Ref 75-77). Consequently, backfield intensity reduces. This, in turn, creates a weaker clamping effect on domain walls (Ref 78, 79). Therefore, the ferroelectric/ferroelastic domain wall switching becomes easier with the increase in grain size in an applied electric field, yielding low E_c values (Ref 75). Since PLZT3_650 film showed improved ferroelectric performance with the variation of process control parameters like annealing temperature and excess Pb, the effect of film thickness was finally studied for same the film on its ferroelectric properties. The improvement in polarization value is observed with increased film thickness with the reduction in E_c and W_{loss} value in the film (Fig. 6e, f), which is desired for a device quality film.

3.4 Room Temperature Switching Current Plot

Figure 7(a) shows the switching current-electric field (I-E) plots of PLZT films. The absence of four switching peaks in the I-E plot suggests the high ferroelectric nature of PLZT films

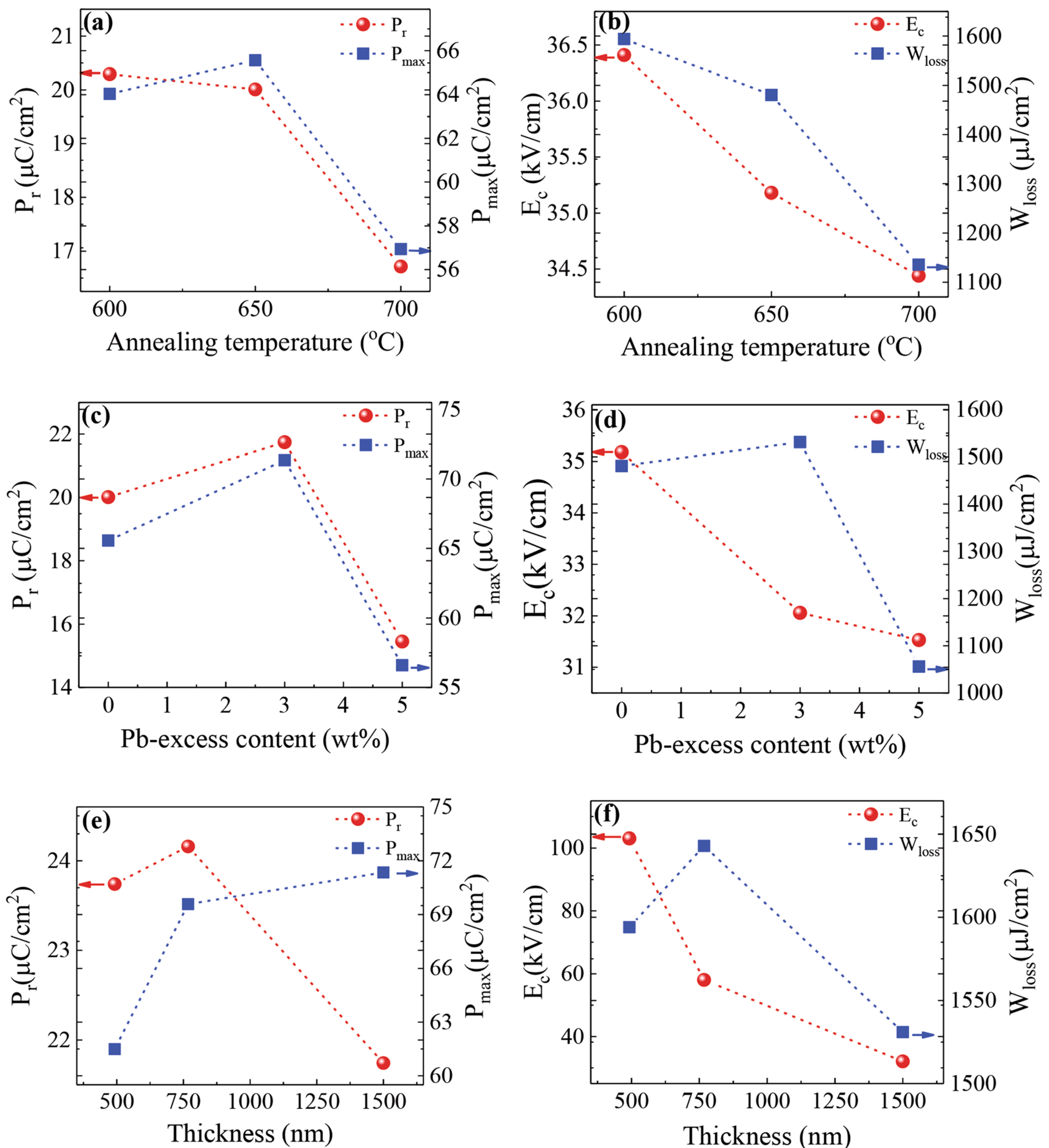

Fig. 6 Effect of process parameters on ferroelectric properties polarization (P_r, P_{max}) coercive field (E_c), and hysteresis loss (W_{loss}) of PLZT: (a, b) effect of annealing temperature (c, d) effect of Pb-excess (e, f) effect of thickness

and is in good agreement with the P-E studies. The I-E plot further confirms the E_c values acquired from PE-loops. That is, at lower electric fields, the developed current is due to the dielectric response of the film. However, as the applied electric field increases, the current value peaks due to domain switching. The current contribution due to domain switching becomes prominent when the domain starts switching after crossing the threshold field. So the electric field corresponding to the maximum switching current in the I-E plot is the film's coercive field (E_c) (Ref 80).

Relatively sharp and intense peaks are obtained for PLZT0_650 film (switching current = 51.5 μA at 45 kV/cm, Fig. 6a). Similar trend is observed in PLZT3 film, showing highest switching current when annealed at 650 °C (Fig. 7b). Among different Pb-excess samples, the sharpest and highly intense switching current peak is obtained for PLZT3_650 film (switching current = 58.10 μA at 40 kV/cm, Fig. 7c). It

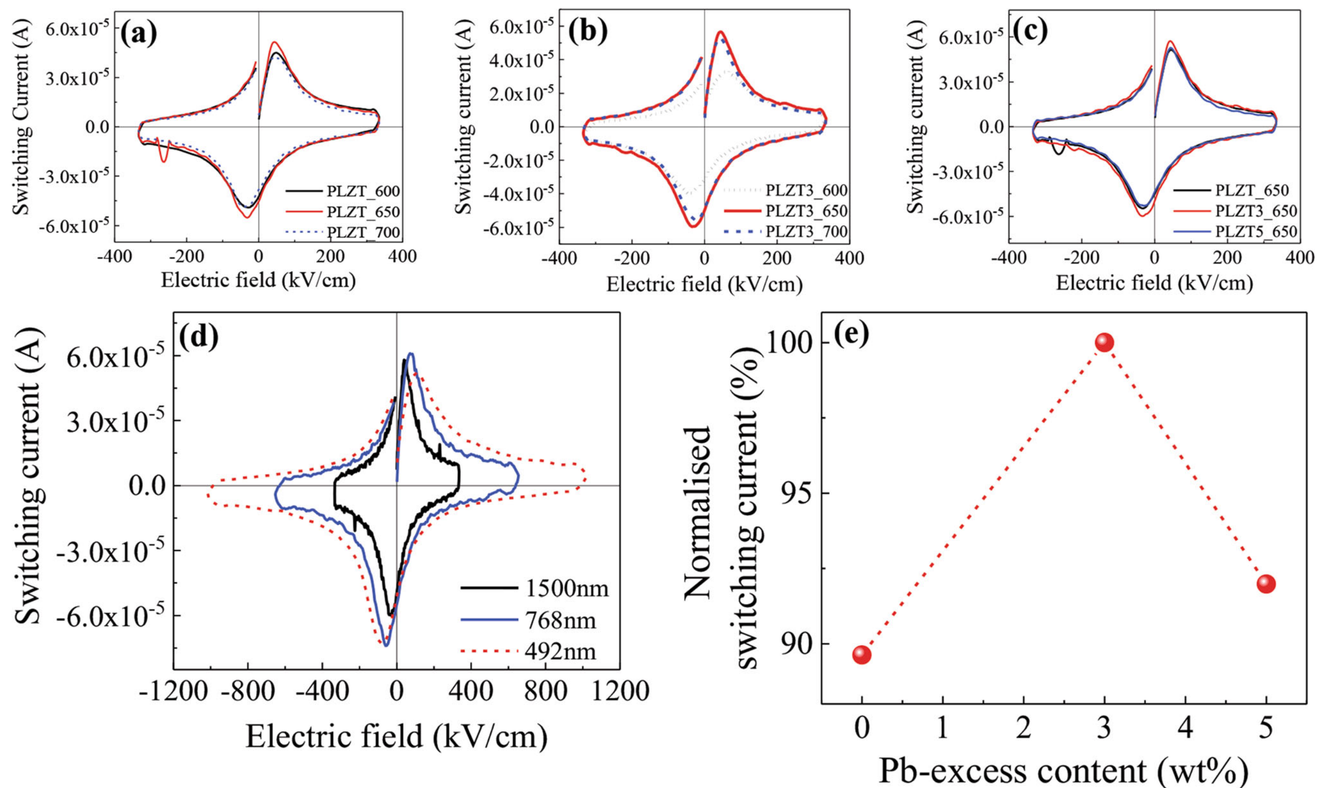

Fig. 7 Effect of process parameters on switching current in PLZT films; (a) annealing temperature on PLZT0, and (b) PLZT3 films, (c) effect of thickness, and (d) normalized switching current with Pb-excess content

indicates the highest domain switching at a slightly lower electric field in PLZT3_650 film, with ~ 10% increment in its switching current value (Fig. 7e). This optimum film is prepared in different thickness and their switching current properties are plotted in Fig. 7d. The 768 nm thick PLZT film showed improved domain switching, at a slightly higher electric field of 70 kV/cm.

3.5 Room Temperature CV Plots

The room temperature C-V plots of PLZT films, measured at an applied voltage of 30 V and an input frequency of 1 kHz, are given in Fig. 8. The corresponding capacitance and dielectric constant values are tabulated in Table 2. The slight difference observed between the two peaks of each film is due to the difference in the top (Ag) and bottom (Pt) electrodes.

The room temperature capacitance value of the films initially increases with an increase in Pb-excess content (Fig. 8c). It corresponds to a very high dielectric value of ~ 2750 in the PLZT3_650 film, which is significantly higher than the previously reported values in other PLZT films (Ref 8, 58, 80-90). This can be correlated with its increased density, larger grain size, and lower percentage of porosity. As the Pb-excess content is further increased to 5 wt.% (PLZT5_650), the capacitance value is reduced. This variation in the capacitance (and dielectric constant) value depending on the Pb-content is associated with the microstructural changes in the film. Along with a higher percentage of porosity in this film, the domain switching current is also verified to be lower in PLZT5_650 film (Sect. 3.4, Fig. 7c). It indicates higher aggregation of point defects at the grain boundaries/domain boundaries, causing domain wall pinning (Ref 91-94). Consequently, the domain wall mobility reduces and correspondingly deteriorates the domain switching current. This pinning of domain walls by point defects causes low permittivity with increasing grain size (Ref 75).

The CV plots of different thickness PLZT films are shown in Fig. 8(d). The zero bias field dielectric constant values of 1500, 768, and 492 nm thick films are ~ 2750, ~ 1680, and 1065, respectively. A similar decrease in dielectric constant value with decreasing film thickness is reported elsewhere (Ref 44, 47, 51, 95). Previous studies suggest that the decrease in the dielectric constant with the decrease in film thickness is due to the formation of a thin layer with a lower dielectric constant, caused by a concentration of space charge carriers such as oxygen vacancies and/or an imperfection induced during film growth, near the film/electrode interfaces (Ref 47-49, 96, 97). However, the current study does not confirm the presence of such a lower dielectric constant layer at the interface. The optimum film, PLZT3_650, showed a dielectric tunability value of 68.46% at an electric field of ~ 200 kV/cm when calculated using the equation below.

$$\tau = (1 - (\varepsilon_r(E)/\varepsilon_r(0)) \times 100\% \quad \text{(Eq 3)}$$

where τ is the tunability, $\varepsilon_r(E)$ is the dielectric constant at an electric field, and $\varepsilon_r(0)$ is the dielectric constant at zero field.

3.6 Room Temperature Leakage Current Plots

The leakage current density of PLZT films increases gradually with the applied voltage. The lowest leakage current density is obtained in PLZT0_650 film (Fig. 9a). Similarly, the 650 °C annealed PLZT3 film shows the lowest leakage current compared to the PLZT3 films annealed at other temperatures

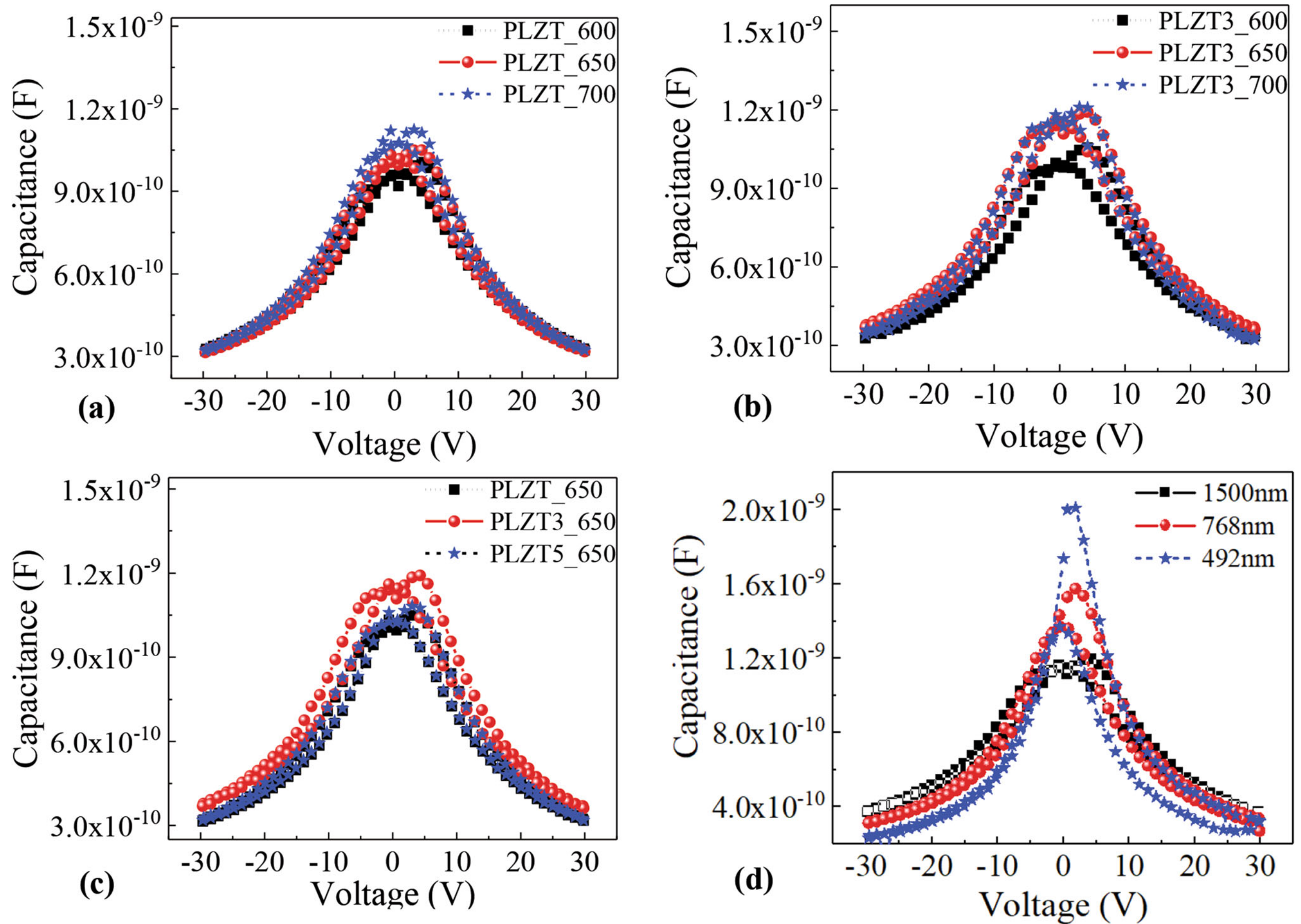

Fig. 8 Effect of process parameters on the capacitance in PLZT film; (a) annealing temperature on PLZT0, and (b) PLZT3 film, (c) effect of Pb-excess, and (d) effect of thickness

Table 2 Room temperature capacitance and dielectric constant value of PLZT films at zero bias field

Sl. no	Sample	Pb-excess, wt.%	Annealing temperature, °C	Thickness, nm	Capacitance, nF	Dielectric CONSTANT
1	PLZT_600	0	600	1500	0.958	2297.23
2	PLZT_650	0	650	1500	1.01	2425.92
3	PLZT_700	0	700	1500	1.07	2565.80
4	PLZT3_600	3	600	1500	0.98	2365
5	PLZT3_650	3	650	1500	1.14	2748.20
6	PLZT3_700	3	700	1500	1.16	2790
7	PLZT5_650	5	650	1500	1.02	2467.38
8	PLZT3	3	650	768	1.36	1680
9	PLZT3	3	650	492	1.73	1065

(Fig. 9b). The comparatively lower leakage current in the PLZT3_650 film (Fig. 9c) is attributed to its reduced porosity (Ref 98–101). In addition, as verified from FESEM images, the PLZT3_650 film has a slightly larger grain size than the PLZT0_650 film. Therefore, the grain boundary density is less in PLZT3_650 film. As a result, defect aggregation at the boundaries is less in PLZT3_650 compared to the PLZT0_ 650 film. This results in less percolating pathways for leakage current. Hence the leakage current is less in the PLZT3_650 film at lower applied voltages (Ref 102–105). Figure 9(d) confirms the reduction in the leakage current density with film thickness. This thickness-dependent arrest in leakage current is responsible for high polarization values in thicker films.

3.7 Room Temperature Energy Storage Plots

The room temperature energy storage density plots of PLZT films are given in Fig. 10. The recoverable energy storage density (W_{rec}), total energy storage density (W_{total}), and energy storage efficiency (η) of the system are calculated using the below equations.

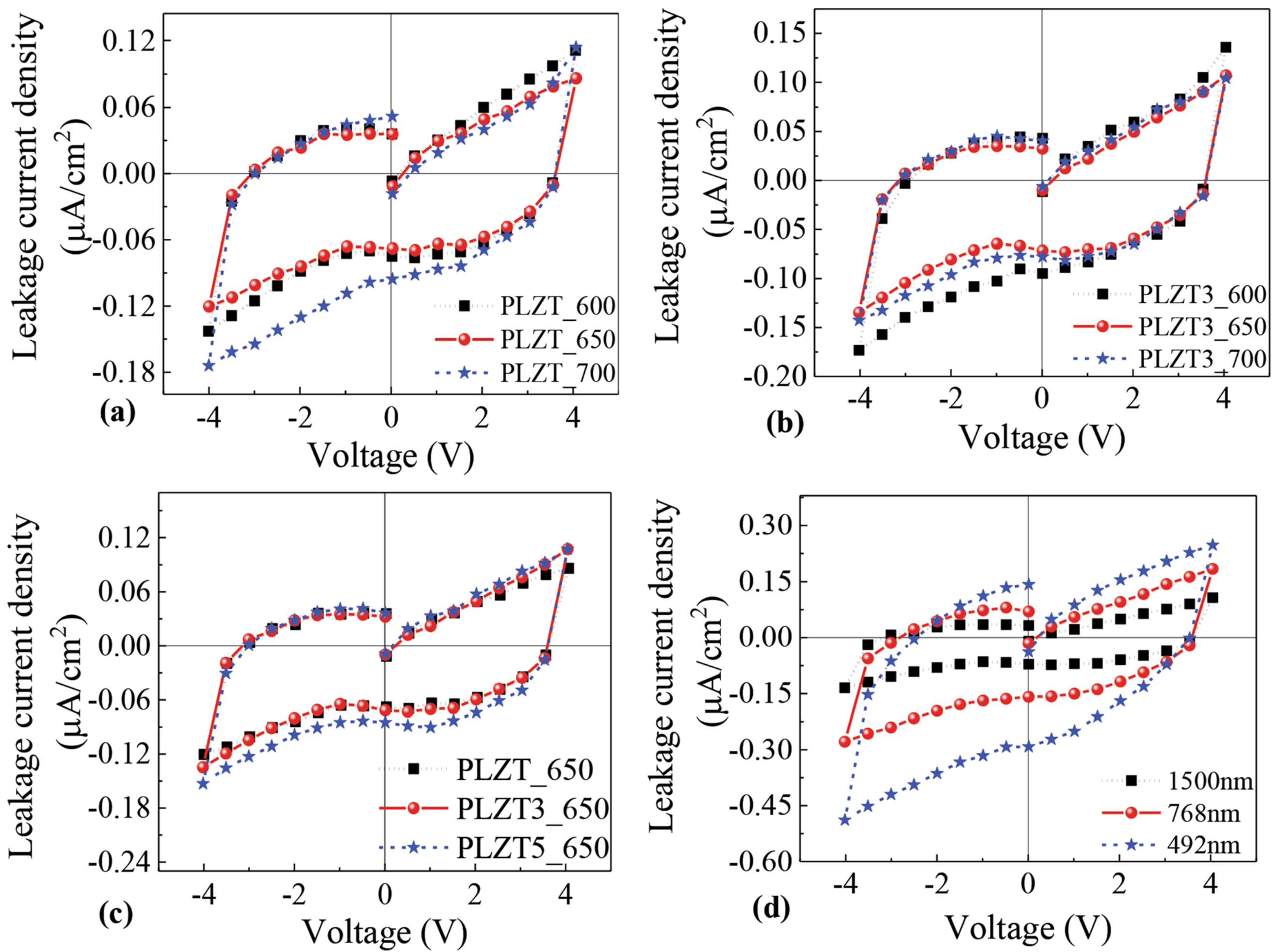

Fig. 9 Effect of process parameters on the room temperature leakage current density in PLZT film; (a) effect of annealing temperature on PLZT0 and (b) PLZT3 film, (c) effect of Pb-excess, and (d) effect of thickness

$$W_{rec} = \int_{P_r}^{P_{max}} EdP \quad \text{(Eq 4)}$$

$$W_{total} = \int_{0}^{P_{max}} EdP \quad \text{(Eq 5)}$$

$$\eta = (W_{rec}/W_{total}) \times 100\% \quad \text{(Eq 6)}$$

where E is the applied electric field. The above calculations are based on the polarization response of the metal/ferroelectric/metal system when an input voltage of 50 V is applied. The annealing temperature study confirmed a maximum W_{rec} value (4.47 J/cm^3 under an electric field of ~ 330 kV/cm) in PLZT0_650 film (Fig. 10a). This can be attributed to the improved crystalline quality and enhanced polarization in the film, which is verified through XRD and hysteresis loop analysis. Figure 10(b) verifies the highest energy storage density in 650 °C annealed PLZT3 film. Figure 10(c) compares the energy storage values of 650 °C annealed PLZT films with different Pb-excess contents. An improved W_{total} (9.45 J/cm^3) and W_{rec} (4.84 J/cm^3) value is observed in the PLZT3_650 film, with the same electric field (~ 330 kV/cm). This is caused by the dense microstructure of PLZT3_650 film, which resulted in lower leakage current density and improved polarization values, as discussed in Sects. 3.2, 3.3, and 3.6.

From Fig. 10(d), it is verified that the energy storage properties improve as the film thickness reduces. It is due to the higher values of the electric field experienced by thinner films. The highest value of W_{total} and W_{rec} obtained are ~ 26 J/cm^3 and ~ 10.50 J/cm^3, respectively, for 492-nm-thick PLZT film under an applied field of ~ 1020 kV/cm.

3.8 Nano-Hardness Test

The nano-indentation test results for the PLZT3 film, annealed at 650 °C are given in Fig. 11 and Table 3. Figure 11 shows the force versus penetration depth plot, obtained from nano-indentation test.

A high Young's modulus value of 143.054 GPa is achieved for PLZT3 film, which is attributed to its good microstructural properties, as discussed in Sect. 3.2 (Fig. 4e).

3.9 Cross-Hatch Adhesion Test

The optical microscope image of cross-hatch adhesion test result revealed totally smooth cutting edges with zero detached square lattices (Fig. 12). It demonstrates the 5B class adherence of the PLZT3 film on $Pt/Ti/SiO_2/Si$ substrate.

Fig. 10 Effect of process parameters on the room temperature energy storage densities in PLZT film; (a) annealing temperature on PLZT0 and (b) PLZT3 film, (c) effect of Pb-excess, and (d) effect of thickness

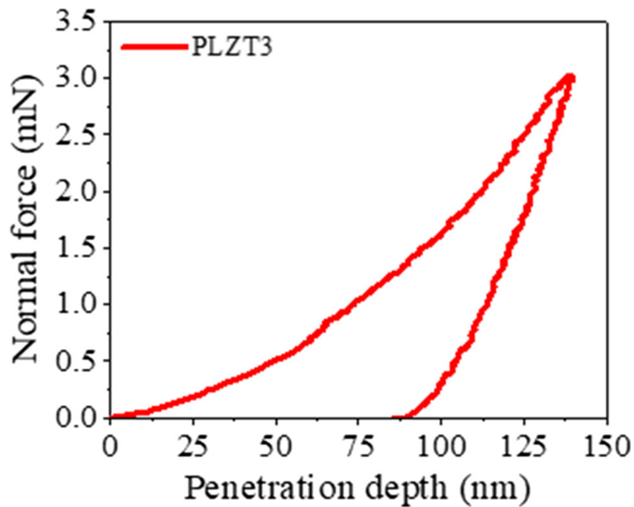

Fig. 11 Normal force vs. penetration depth plot of PLZT3 film

4. Conclusions

Effect of process parameters (annealing temperature, Pb-excess content, and film thickness) on structure, microstructure, dielectric and ferroelectric properties of PLZT film, prepared by chemical solution deposition was investigated in the present study. At first, the effect of annealing temperature (600, 625, 650, 675, and 700 °C) and Pb-excess (0, 1, 2, 3, and 5 wt.%) content in the structural properties of PLZT films were studied. Results showed high crystallinity and orientation for 650 °C annealed films, which resulted in improved ferroelectric properties like better domain switching, low leakage current densities, and improved energy storage densities compared to the other PLZT films annealed at 600, 625, 675, and 700 °C. The 3 wt.% Pb-excess composition (PLZT3_650 film) yielded the highest domain switching (~ 10% increment), low leakage current density, high dielectric constant (~ 2750), and improved energy storage density (W_{total} = 0.9.45 J/cm^3 under

Table 3 Nano-indentation measurement results of PLZT films

Film	Pb-excess, wt.%	Annealing temperature, °C	Hardness, MPa	Young's modulus, GPa
PLZT3	3	650	7894.430	143.054

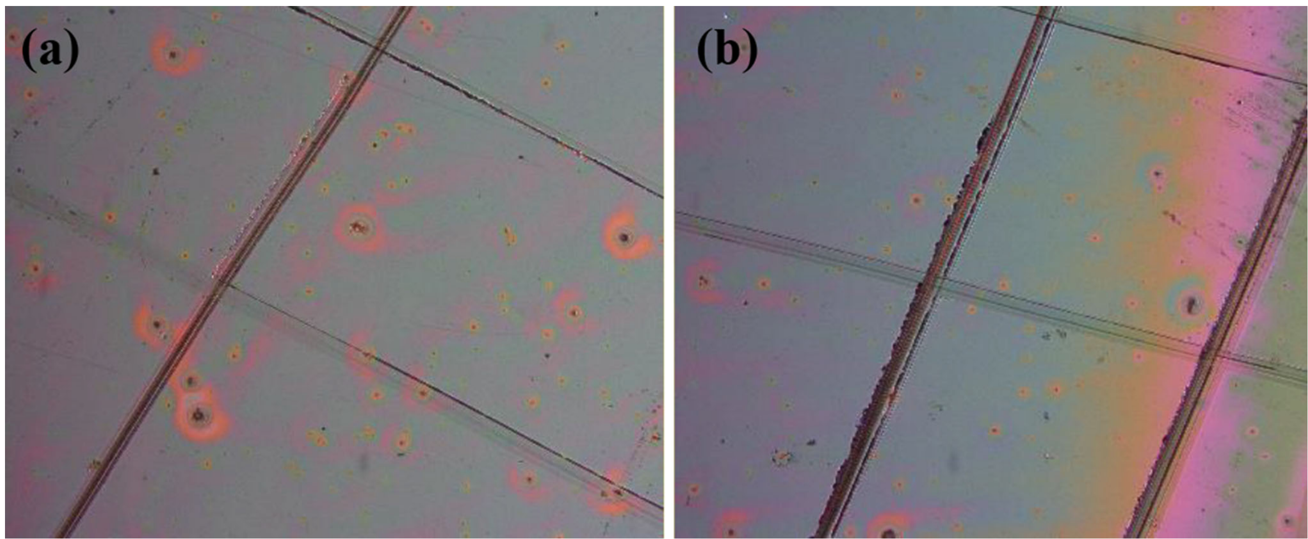

Fig. 12 Optical microscope images of cross-hatch adhesion test result

330 kV/cm). In addition, the film exhibited strong polarization (P_{max} = 71.4 μC/cm^2 at 334 kV/cm) as a result of its improved microstructural density and larger volume fraction of polarization domains. The optimum film, PLZT3_650 showed a hardness value of 7894.43 MPa, Young's modulus value of 143.05GPa, and an ASTM class 5B adhesion on the substrate. Finally, the thickness study (492 nm, 768 nm, and 1500 nm) on the optimum composition PLZT3_650 showed better ferroelectric and dielectric properties due to the reduction in leakage current. The maximum energy storage density (W_{total} = $\sim$ 26 J/cm^3 at 1020 kV/cm) was obtained for PLZT3_650 film.

Acknowledgment

The authors acknowledge the research facilities and infrastructure from CSIR-National Aerospace Laboratories. A.A.B acknowledges the doctoral fellowship from CSIR, India, and AcSIR, Ghaziabad, for the Ph.D. position to carry out the research.

References

1. C. Huang et al., Large Quadratic Electro-Optic Effect of the PLZT Thin Films for Optical Communication Integrated Devices, *ACS Photonics*, 2020, **7**(11), p 3166–3176
2. X. Niu et al., High-Performance PZT-Based Stretchable Piezoelectric Nanogenerator, *ACS Sustain. Chem. Eng.*, 2018, **7**(1), p 979–985
3. W.Y. Pan, C.Q. Dam, Q.M. Zhang, and L.E. Cross, Large Displacement Transducers Based on Electric Field Forced Phase Transitions in the Tetragonal ($Pb_{0.97}La_{0.02}$(Ti.Zr.Sn)O_3 Family of Ceramics, *J. Appl. Phys.*, 1989, **66**, p 6014–6023
4. M.D. Nguyen, E.P. Houwman, M.T. Do, and G. Rijnders, Relaxor-Ferroelectric Thin Film Heterostructure with Large Imprint for High energy-Storage Performance at Low Operating Voltage, *Energy Storage Mater.*, 2020, **25**, p 193–201
5. M.S. Mirshekarioo, K. Yao, and T. Sirtharan, Large Strain and High Energy Storage Density in Orthorhombic Perovskite ($Pb_{0.97}La_{0.02}$) (Zr_{1-x-y}SnxTiy)O_3 Antiferroelectric Thin Films, *Appl. Phys. Lett.*, 2010, **97**, p 142902
6. B. Peng et al., Large Energy Storage Density and High Thermal Stability in a Highly Textured (111)-Oriented $Pb_{0.8}Ba_{0.2}ZrO_3$ Relaxor Thin Film with the Coexistence of Antiferroelectric and ferroelecTric Phases, *ACS Appl. Mater. Interfaces*, 2015, **7**(24), p 13512–13517
7. K. Yao et al., Nonlinear Dielectric Thin Films for High-Power Electric Storage with Energy Density Comparable with Electrochemical Supercapacitors, *IEEE Trans. Ultrason. Ferroelectr. Freq. Control*, 2011, **58**(9), p 1968–1974
8. X. Hao, Y. Wang, J. Yang, S. An, and J. Xu, High Energy-Storage Performance in $Pb_{0.91}La_{0.09}(Ti_{0.65}Zr_{0.35})O_3$ Relaxor Ferroelectric Thin Films, *J. Appl. Phys.*, 2012, **112**(11), p 114111
9. B.P. Bruno, A.R. Fahmy, M. Stürmer, U. Wallrabe, and M.C. Wapler, Properties of Piezoceramic Materials in High Electric Field Actuator Applications, *Smart Mater. Struct.*, 2018, **28**(1), p 015029
10. X. Wang, J. Shen, T. Yang, Y. Dong, and Y. Liu, High Energy-Storage Performance and Dielectric Properties of Antiferroelectric $(Pb_{0.97}La_{0.02})(Zr_{0.5}Sn_{0.5-x}Ti_x)O_3$ Ceramic, *J. Alloys Compd.*, 2016, **655**, p 309–313
11. G. Zhang et al., High-Energy Storage Performance of $(Pb_{0.87}Ba_{0.1}La_{0.02})(Zr_{0.68}Sn_{0.24}Ti_{0.08})O_3$ Antiferroelectric Ceramics Fabricated by the Hot-Press Sintering Method, *J. Am. Ceram. Soc.*, 2015, **98**, p 1175–1181
12. X.L. Wang, L. Zhang, X.H. Hao, and S.L. An, High Energy-Storage Performance of 0.9Pb $(Mg_{1/3}Nb_{2/3})O_3$-0.1$PbTiO_3$ Relaxor Ferroelectric Thin Films Prepared by RF Mag- Netron Sputtering, *Mater. Res. Bull.*, 2015, **65**, p 73–79
13. C.T. Nguyen, H.N. Vu, and M.D. Nguyen, High-Performance Energy Storage and Breakdown Strength of Low-Temperature Laser-Deposited Relaxor PLZT Thin Films on Flexible Ti-Foils, *J. Alloys Compd.*, 2019, **802**, p 422–429
14. H. Tang, Y. Lin, C. Andrews, and H.A. Sodano, Nanocomposites with Increased Energy Density Through High Aspect Ratio PZT Nanowires, *Nanotechnology*, 2011, **22**, p 015702–015711
15. Q. Zhang et al., High Recoverable Energy Density over a Wide Temperature Range in Sr Modified (Pb.La)(Zr.Sn.Ti)O_3 Antiferroelectric Ceramics with an Orthorhombic Phase, *Appl. Phys. Lett.*, 2016, **109**, p 262901
16. L. Zhang, S. Jiang, B. Fan, and G. Zhang, High Energy Storage Performance in $(Pb_{0.858}Ba_{0.1}La_{0.02}Y_{0.008})(Zr_{0.65}Sn_{0.3}Ti_{0.05})O_3$-$(Pb_{0.97}La_{0.02})(Zr_{0.9}Sn_{0.05}Ti_{0.05})O_3$ Anti-Ferroelectric Composite Ceramics, *Ceram. Int.*, 2015, **41**(1), p 1139–1144
17. Y.Z. Li, Z.J. Wang, Y. Bai, and Z.D. Zhang, High Energy Storage Performance in Ca-doped $PbZrO_3$ Antiferroelectric Films, *J. Eur. Ceram. Soc.*, 2020, **40**(4), p 1285–1292
18. D. Oliveira, M.A.A.V. Monteiro, and J.V. Filho, A New Structural Health Monitoring Strategy Based on PZT Sensors and Convolutional Neural Network, *Sensors.*, 2018, **18**(9), p 2955
19. J. Li et al., A Walking Type Piezoelectric Actuator Based on the Parasitic Motion of Obliquely Assembled PZT Stacks, *Smart Mater. Struct.*, 2021, **30**(8), p 085030
20. G. Lu, Y. Li, M. Zhou, Q. Feng, and G. Song, Detecting Damage Size and Shape in a Plate Structure Using PZT Transducer Array, *J. Aerosp. Eng.*, 2018, **31**(5), p 04018075

21. Y. Zhang et al., Enhanced Pyroelectric and Piezoelectric Properties of PZT with Aligned Porosity for Energy Harvesting Applications, *J. Mater. Chem. A*, 2017, **5**(14), p 6569–6580
22. Y. Li et al., Flexible PLZT Antiferroelectric Film Capacitor for Energy Storage in Wide Temperature Range, *J. Alloys Compd.*, 2021, **868**, p 159129
23. P. Qiao, Y. Zhang, X. Chen, M. Zhou, G. Wang, and X. Dong, Effect of Mn-doping on Dielectric and Energy Storage Properties of $(Pb_{0.91}La_{0.06})(Zr_{0.96}Ti_{0.04})O_3$ Antiferroelectric Ceramics, *J. Alloys Compd.*, 2019, **780**, p 581–587
24. H. Wu et al., Effect of Holding Time on Microstructure Ferroelectric and Energy-Storage Properties of $Pb_{0.925}La_{0.05}Zr_{0.95}Ti_{0.05}O_3$@$SiO_2$ Ceramics, *J. Alloys Compd.*, 2022, **896**, p 162932
25. X. Qin et al., Enhanced Energy-Storage Performance of $Pb_{0.925}La_{0.05}Zr_{0.95}Ti_{0.05}$@ x wt.%$SiO_2$ Composite Ceramics, *J. Alloys Compd.*, 2022, **890**, p 161869
26. M. Kumar, G. Sharma, S.D. Kaushik, A.K. Singh, and S. Kumar, Critical Behavior of Relaxor $Pb_{0.91}La_{0.09}Zr_{0.65}Ti_{0.35}O_3$: Interplay Between Polar Nano Regions, Electrocaloric and Energy Storage Response, *J. Alloys Compd.*, 2021, **884**, p 161067
27. J. Wang, Z.G. Wu, X.M. Yuan, S.R. Jiang, and P.X. Yan, The Effect of Heat-Treatment on the Structure and Chemical Homogeneity of Ferroelectrics PLZT Thin Films Deposited by RF Sputtering, *Mater. Chem. Phys.*, 2004, **88**(1), p 77–83
28. M.D. Nguyen, C.T. Nguyen, H.N. Vu, and G. Rijnders, Controlling Microstructure and Film Growth of Relaxor-Ferroelectric Thin Films for High Break-Down Strength and Energy-Storage Performance, *J. Eur. Ceramic Soc.*, 2018, **38**(1), p 95–103
29. A.A. Jeyaseelan and S. Dutta, Improvement in Piezoelectric Properties of PLZT Thin Film with Large Cation Doping at A-Site, *J. Alloys Compd.*, 2020, **826**, p 153956
30. G. Chen et al., Effects of the Film Thickness and Poling Electric Field on Photovoltaic Performances of $(Pb.La)(Zr.Ti)O_3$ Ferroelectric Thin Film-Based Devices, *Ceram. Int.*, 2020, **46**(4), p 4148–4153
31. A. Anju Balaraman and S. Dutta, Inorganic Dielectric Materials for Energy Storage Applications: A Review, *J. Phys. D Appl. Phys.*, 2022, **55**(18), p 183002
32. B. Ma, Z. Hu, S. Liu, M. Narayanan, and U. Balachandran, Temperature Dependent Polarization Switching Properties of Ferroelectric $Pb_{0.92}La_{0.08}Zr_{0.52}Ti_{0.48}O\delta$ Films Grown on Nickel Foils, *Appl. Phys. Lett.*, 2013, **102**(7), p 072901
33. S. Hong. *Nanoscale phenomena in ferroelectric thin films*. 2004
34. G.H. Haertling, Ferroelectric Thin Films for Electronic Applications, *J. Vac. Sci. Technol. A: Vac. Surfaces Films*, 1991, **9**(3), p 414–420
35. F. Wang, D. Meng, X. Li, Z. Zhu, Z. Fu, and Y. Lu, Influence of Annealing Temperature on the Crystallization and Ferroelectricity of Perovskite CH3NH3PbI3 Film, *Appl. Surface Sci.*, 2015, **357**, p 391–396
36. P.D. Lomenzo, Q. Takmeel, S. Moghaddam, and T. Nishida, Annealing Behavior of Ferroelectric Si-Doped HfO_2 Thin Films, *Thin Solid Films.*, 2016, **615**, p 139–144
37. Z. Lin, W. Cai, W. Jiang, C. Fu, C. Li, and Y. Song, Effects of Annealing Temperature on the Microstructure, Optical, Ferroelectric and Photovoltaic Properties of $BiFeO_3$ Thin Films Prepared by Sol–Gel Method, *Ceram. Int.*, 2013, **39**(8), p 8729–8736
38. E. R. Myers and A. I. Kingon Ferroelectric Thin Films, in *Materials Research Society Symposium Proceedings*. 1990. p. Volume 200
39. E.B. Araujo et al., Processing and Structural Properties of Random Oriented Lead Lanthanum Zirconate Titanate Thin Films, *Mater. Res. Bull.*, 2015, **61**, p 26–31
40. G.L. Brennecka and B.A. Tuttle, Fabrication of Ultrathin Film Capacitors by Chemical Solution Deposition, *J. Mater. Res.*, 2007, **22**(10), p 2868–2874
41. A.P. Wilkinson, J.S. Speck, A.K. Cheetham, S. Natarajan, and J.M. Thomas, In Situ X-Ray Diffraction Study of Crystallization Kinetics in PbZr1−xTixO_3,(PZT, x = 0, 055, 1.0), *Chem. Mater.*, 1994, **6**(6), p 750–754
42. A.Z. Simoes, A.H.M. Gonzalez, M.A. Zaghete, J.A. Varela, and B.D. Stojanovic, Effects of Annealing on the Crystallization and Roughness of PLZT Thin Films, *Thin Solid Films.*, 2001, **384**(1), p 132–137
43. S. Kandasamy et al., Heat Treatment Effects on the Formation of Lanthanum-Modified Lead Zirconate Titanate Thin Films, *Mater. Lett.*, 2008, **62**(3), p 370–373
44. G.H. Haertling, Thickness Dependent Properties of Acetate-Derived PLZT Films, *Integr. Ferroelectr.*, 1997, **14**(1–4), p 219–228
45. H. Pan, Y. Zeng, Y. Shen, Y.-H. Lin, and C.-W. Nan, Thickness-Dependent Dielectric and Energy Storage Properties of $(Pb_{0.96}La_{0.04})(Zr_{0.98}Ti_{0.02})O_3$ Antiferroelectric Thin Films, *J. Appl. Phys.*, 2016, **119**(12), p 124106
46. C. Neusel, H. Jelitto, D. Schmidt, R. Janßen, F. Felten, and G.A. Schneider, Thickness-Dependence of the Breakdown Strength: Analysis of the Dielectric and Mechanical Failure, *J. Eur. Ceram. Soc.*, 2015, **35**(1), p 113–123
47. M.D. Nguyen, D.T. Tran, H.T. Dang, C.T. Nguyen, G. Rijnders, and H.N. Vu, Relaxor-Ferroelectric Films for Dielectric Tunable Applications: Effect of Film Thickness and Applied Electric Field, *Materials*, 2021, **14**(21), p 6448
48. J. Oh et al., The Dependence of Dielectric Properties on the Thickness of (Ba.Sr) TiO_3 Thin Films, *Curr. Appl. Phys.*, 2007, **7**(2), p 168–171
49. J. Pérez De La Cruz, E. Joanni, P.M. Vilarinho, and A.L. Kholkin, Thickness Effect on the Dielectric, Ferroelectric, and Piezoelectric Properties of Ferroelectric Lead Zirconate Titanate Thin Films, *J. Appl. Phys.*, 2010, **108**(11), p 114106
50. X. Hao, J. Zhai, F. Zhou, X. Song, and S. An, Thickness and Frequency Dependence of Electric-Field-Induced Strains of Sol-Gel Derived $(Pb_{0.97}La_{0.02})(Zr_{0.95}Ti_{0.05})O_3$ Antiferroelectric Films, *J. Sol-gel Sci. Technol.*, 2010, **53**(2), p 366–371
51. K. Natori, D. Otani, and N. Sano, Thickness Dependence of the Effective Dielectric Constant in a Thin Film Capacitor, *Appl. Phys. Lett.*, 1998, **73**(5), p 632–634
52. M. Avrami, Granulation, Phase change, and Microstructure Kinetics of Phase Change. III, *J. Chem. Phys.*, 1941, **9**(2), p 177–184
53. E. Fatuzzo, Theoretical Considerations on the Switching Transient in Ferroelectrics, *Phys. Rev.*, 1962, **127**(6), p 1999
54. Y. Ishibashi and Y. Takagi, Note on ferroelectric domain switching, *J. Phys. Soc. Jpn.*, 1971, **31**(2), p 506–510
55. V. Gopalan and T.E. Mitchell, In Situ Video Observation of 180 Domain Switching in $LiTaO_3$ by Electro-Optic Imaging Microscopy, *J. Appl. Phys.*, 1991, **85**(4), p 2304–2311
56. R. Gaynutdinov, S. Yudin, S. Ducharme, and V. Fridkin, Homogeneous Switching in Ultrathin Ferroelectric Films, *J. Phys. Condens. Matter*, 2011, **24**(1), p 015902
57. M.J. Zou, Y.L. Tang, Y.P. Feng, W.R. Geng, X.L. Ma, and Y.L. Zhu, Influence of Flexoelectric Effects on Domain Switching in Ferroelectric Films, *J. Appl. Phys.*, 2021, **129**(18), p 184103
58. Z. Hu, B. Ma, S. Liu, M. Narayanan, and U. Balachandran, Relaxor Behavior and Energy Storage Performance of Ferroelectric PLZT Thin Films with Different Zr/Ti Ratios, *Ceram. Int.*, 2014, **40**(1), p 557–562
59. B. Ma, S. Liu, S. Tong, M. Narayanan, and U. Balachandran, Enhanced Dielectric Properties of $Pb_{0.92}La_{0.08}Zr_{0.52}Ti_{0.48}O_3$ Films with Compressive Stress, *J. Appl. Phys.*, 2012, **112**(11), p 114117
60. S. Tong et al., Effect of Lanthanum Content and Substrate Strain on Structural and Electrical Properties of Lead Lanthanum Zirconate Titanate thin Films, *Mater. Chem. Phys.*, 2013, **140**(2–3), p 427–430
61. W. Xu, Q. Li, Z. Yin, X. Wang, and H. Zou, Effect of La Doping on Crystalline Orientation, Microstructure and Dielectric Properties of PZT Thin Films, *Mater. Test.*, 2017, **59**(10), p 885–889
62. A. Antony Jeyaseelan and S. Dutta, Effect of Ligand Concentration on Microstructure, Ferroelectric and Piezoelectric Properties of PLZT Film, *Mater. Chem. Phys.*, 2015, **162**, p 487–490
63. N. Md, Impact of Fatigue Behavior on Energy Storage Performance in Dielectric Thin-Film Capacitors, *J. Eur. Ceram. Soc.*, 2020, **40**(5), p 1886–1895
64. A. Pandey, S. Dalal, S. Dutta, and A. Dixit, Structural Characterization of Polycrystalline Thin Films by X-ray Diffraction Techniques, *J. Mater. Sci.: Mater. Electron.*, 2021, **32**, p 1341–1368
65. F. Vassenden, G. Linker, and J. Geerk, Growth Direction Control YBCO Thin Films, *Physica C*, 1991, **175**(5–6), p 566–572
66. T. Nakamura, Y. Yamada, T. Kusumori, H. Minoura, and H. Muto, Improvement in the Crystallinity of ZnO Thin Films by Introduction of a Buffer Layer, *Thin Solid Films*, 2002, **411**(1), p 60–64
67. N. Jackson, F. Stam, J. O'Brien, L. Kailas, A. Mathewson, and C. O'Murchu, Crystallinity and Mechanical Effects From Annealing Parylene Thin Films, *Thin Solid Films*, 2016, **603**, p 371–376
68. M. Toyoda, Y. Nanbu, Y. Nakazawa, M. Hirano, and M. Inagaki, Effect of Crystallinity of Anatase on Photoactivity for Methyleneblue

Decomposition in Water, *Appl. Catal. B Environ.*, 2004, **49**(4), p 227–232

69. X. Hao, J. Zhou, and S. An, Effects of PbO Content on the Dielectric Properties and Energy Storage Performance of $(Pb_{0.97}La_{0.02})(Zr_{0.97}Ti_{0.03})O_3$ Antiferroelectric Thin Films, *J. Am. Ceram. Soc.*, 2011, **94**(6), p 1647–1650
70. S. Gariglio, N. Stucki, J.-M. Triscone, and G. Triscone, Strain relaxation and critical temperature in epitaxial ferroelectric Pb $(Zr_{0.20}Ti_{0.80})O_3$ thin films, *Appl. Phys. Lett.*, 2007, **90**(20), p 202905
71. Z. Zhao et al., Grain-Size Effects on the Ferroelectric Behavior of Dense Nanocrystalline $BaTiO_3$ Ceramics, *Phys. Rev. B*, 2004, **70**(2), p 024107
72. M.D. Nguyen, Tuning the Energy Storage Performance, Piezoelectric Strain and Strain Hysteresis of Relaxor PLZT Thin Films Through Controlled Microstructure by Changing the Ablation Rate, *J. Eur. Ceram. Soc.*, 2019, **39**(6), p 2076–2081
73. S.J. Kang and Y.H. Joung, Fatigue, Retention and Switching Properties of PLZT (x/30/70) Thin Films with Various La Concentrations, *J. Mater. Sci.*, 2007, **42**(18), p 7899–7905
74. G. Viola, K. Boon Chong, F. Guiu, and M. John Reece, Role of Internal Field and Exhaustion in Ferroelectric Switching, *J. Appl. Phys.*, 2014, **115**(3), p 034106
75. Y. Tan et al., Unfolding Grain Size Effects in Barium Titanate Ferroelectric Ceramics, *Sci. Rep.*, 2015, **5**(1), p 1–9
76. M. Eriksson et al., Ferroelectric Domain Structures and Electrical properties of Fine-Grained Lead-Free Sodium potassium Niobate Ceramics, *J. Am. Ceram. Soc.*, 2011, **94**(10), p 3391–3396
77. J.-F. Chou, M.-H. Lin, and H.-Y. Lu, Ferroelectric Domains in Pressureless-Sintered Barium Titanate, *Acta Mater.*, 2000, **48**(13), p 3569–3579
78. W. Cao, The Strain Limits on Switching, *Nat. Mater.*, 2005, **4**(10), p 727–728
79. H.T. Martirena and J.C. Burfoot, Grain-Size Effects on Properties of Some Ferroelectric Ceramics, *J. Phys. C Solid State Phys.*, 1974, **7**(17), p 3182
80. A. Kumar, S.R. Emani, K.C.J. Raju, J. Ryu, and A.R. James, Investigation of the Effects of Reduced Sintering Temperature on Dielectric, Ferroelectric and Energy Storage Properties of Microwave-Sintered PLZT 8/60/40 Ceramics, *Energies*, 2020, **13**(23), p 6457
81. M.D. Nguyen, C.T. Nguyen, H.N. Vu, and G. Rijnders, Experimental Evidence of Breakdown Strength and its Effect on Energy-Storage Performance in Normal and Relaxor Ferroelectric Films, *Curr. Appl. Phys.*, 2019, **19**(9), p 1040–1045
82. M.D. Nguyen, E.P. Houwman, and G. Rijnders, Energy Storage Performance and Electric Breakdown Field of Thin Relaxor Ferroelectric PLZT Films Using Microstructure and Growth Orientation Control, *J. Phys. Chem. C*, 2018, **122**(27), p 15171–15179
83. T. Hirano, H. Kawai, H. Suzuki, S. Kaneko, and A. Wada, Effect of Excess Lead Addition on Processing of Sol-Gel Derived Lanthanum-Modified Lead Zirconate Titanate Thin Film, *Jpn. J. Appl. Phys.*, 1999, **38**(9S), p 5354
84. S. Tong et al., Lead Lanthanum Zirconate Titanate Ceramic Thin Films for Energy Storage, *ACS Appl. Mater. Interfaces*, 2013, **5**(4), p 1474–1480
85. B. Ma et al., Residual Stress of $(Pb_{0.92}La_{0.08})(Zr_{0.52}Ti_{0.48})O_3$ Films Grown by a Sol–Gel Process, *Smart Mater. Struct.*, 2013, **22**(5), p 055019
86. C. Vijayaraghavan, T.C. Goel, and R.G. Mendiratta, Structural and Electrical Properties of Sol-Gel Synthesized PLZT Thin Films, *IEEE Trans. Dielectr. Electr. Insul.*, 1999, **6**(1), p 69–72
87. Y. Zhao, X. Hao, and Q. Zhang, Energy-Storage Properties and Electrocaloric Effect of Pb (1–3 x/2) La x $Zr_{0.85}Ti_{0.15}O_3$ Antiferroelectric Thick Films, *ACS Appl. Mater. Interfaces*, 2014, **6**(14), p 11633–11639
88. M.D. Nguyen, E.P. Houwman, M. Dekkers, C.T. Nguyen, H.N. Vu, and G. Rijnders, Research Update: Enhanced Energy Storage Density and Energy Efficiency of Epitaxial $Pb_{0.9}La_{0.1}(Zr_{0.52}Ti_{0.48})O_3$ Relaxor-Ferroelectric Thin-Films Deposited on Silicon by Pulsed Laser Deposition, *APL Mater.*, 2016, **4**(8), p 080701
89. E. Brown, C. Ma, J. Acharya, B. Ma, J. Wu, and J. Li, Controlling Dielectric and Relaxor-Ferroelectric Properties for Energy Storage by tuning $Pb_{0.92}La_{0.08}Zr_{0.52}Ti_{0.48}O_3$ Film Thickness, *ACS Appl. Mater. Interfaces*, 2014, **6**(24), p 22417–22422
90. B. Ma, D.-K. Kwon, M. Narayanan, and U. Balachandran, Dielectric Properties and Energy Storage Capability of Antiferroelectric $Pb_{0.92}La_{0.08}Zr_{0.95}Ti_{0.05}O_3$ Film-on-Foil Capacitors, *J. Mater. Res.*, 2009, **24**, p 2993
91. I. K. Yoo and S. B. Desu., "Fatigue parameters of lead zirconate titanate thin films, in *MRS Online Proceedings Library (OPL)*, 1991, p. 243
92. J.F. Scott and C.A.P. de Araujo, Ferroelectric Memories, *Science*, 1989, **246**(4936), p 1400–1405
93. L. He and D. Vanderbilt, First-Principles Study of Oxygen-Vacancy Pinning of Domain Walls in $PbTiO_3$, *Phys. Rev. B*, 2003, **68**(13), p 134103
94. Y.-K. Choi, T. Hoshina, H. Takeda, and T. Tsurumi, Effect of Oxygen Vacancy and Oxygen Vacancy Migration on Dielectric Response of $BaTiO_3$-Based Ceramics, *Jpn. J. Appl. Phys.*, 2011, **50**, p 031504
95. C.S. Hwang, Thickness-Dependent Dielectric Constants of (Ba, Sr) TiO_3 Thin Films with Pt or Conducting Oxide Electrodes, *J. Appl. Phys.*, 2002, **92**(1), p 432–437
96. T.M. Doan, L. Lu, and M.O. Lai, Thickness Dependence of Structure, Tunable and Pyroelectric Properties of Laser-Ablated Ba $(Zr_{0.25}Ti_{0.75})O_3$ Thin Films, *J. Phys. D. Appl. Phys.*, 2010, **43**(3), p 035402
97. S. Song, J. Zhai, L. Gao, X. Yao, S. Lu, and Z. Xu, Thickness-Dependent Dielectric and Tunable Properties of Barium stannate Titanate Thin Films, *J. Appl. Phys.*, 2009, **106**(2), p 024104
98. H. Yang, F. Yan, Y. Lin, T. Wang, L. He, and F. Wang, A Lead Free Relaxation and High Energy Storage Efficiency Ceramics for Energy Storage Applications, *J. Alloys Compd.*, 2017, **710**, p 436
99. Y. Podgorny, K. Vorotilov, P. Lavrov, and A. Sigov, Leakage Currents in Porous PZT Films, *Ferroelectrics*, 2016, **503**(1), p 77–84
100. P. Shi et al., Study on the Properties of Pb (Zr, Ti)O_3 Thin Films Grown Alternately by Pulsed Laser Deposition and Sol-Gel Method, *Phys. Lett. A*, 2020, **384**(11), p 126232
101. C.M. Raghavan, J.W. Kim, and S.S. Kim, Effects of Ho and Ti Doping on Structural and Electrical Properties of $BiFeO_3$ Thin Films, *J. Am. Ceram. Soc.*, 2014, **97**(1), p 235–240
102. J. Narayan, R.A. Weeks, and E. Sonder, Aggregation of Defects and Thermal-Electric Breakdown in MgO, *J. Appl. Phys.*, 1978, **49**(12), p 5977–5981
103. K. Kukli et al., Properties of Hafnium Oxide Films Grown by Atomic Layer Deposition from Hafnium Tetraiodide and Oxygen, *J. Appl. Phys.*, 2002, **92**(10), p 5698–5703
104. K. McKenna et al., Grain Boundary Mediated Leakage Current in Polycrystalline HfO_2 Films, *Microelectron. Eng.*, 2011, **88**(7), p 1272–1275
105. K. Murakami, M. Rommel, V. Yanev, A.J. Bauer, and L. Frey, Current Voltage Characteristics through Grains and Grain Boundaries of High-k Dielectric Thin Films Measured by Tunneling Atomic Force Microscopy, *AIP Conf. Proc.*, 2011, **1395**, p 134–138

Publisher's Note Springer Nature remains neutral with regard to jurisdictional claims in published maps and institutional affiliations.

Springer Nature or its licensor (e.g. a society or other partner) holds exclusive rights to this article under a publishing agreement with the author(s) or other rightsholder(s); author self-archiving of the accepted manuscript version of this article is solely governed by the terms of such publishing agreement and applicable law.